A novel Munc13-4/S100A10/Annexin A2 complex promotes Weibel-Palade body exocytosis in endothelial cells

Tarek Chehab*†, Nina Criado Santos*†, Anna Holthenrich†, Sophia N. Koerdt†, Jennifer Disse†, Christian Schuberth‡, Ali Reza Nazmi†, Maaike Neeft§, Henriette Koch||, Kwun Nok M. Man||, Sonja M. Wojcik||, Thomas F. J. Martin¶, Peter van der Sluijs$, Nils Brose||, Volker Gerke†

†Institute of Medical Biochemistry,
‡Institute of Cell Dynamics and Imaging,
Centre for Molecular Biology of Inflammation (ZMBE),
Cells-in-Motion Cluster of Excellence (EXC 1003 – CiM), University of Münster
Von-Esmarch-Str. 56, 48149 Münster, Germany

§Department of Cell Biology, Center of Molecular Medicine, University Medical Center Utrecht, 3584 CX Utrecht, The Netherlands.

||Max Planck Institute of Experimental Medicine, Department of Molecular Neurobiology, Hermann-Rein-Straße 3, 37075 Göttingen, Germany.

¶Department of Biochemistry, University of Wisconsin-Madison, 433 Babcock Drive, Madison, WI 53706, USA.

*equally contributing authors

Running head: Munc13-4 in Weibel-Palade body exocytosis

Key words: Blood coagulation, Ca^{2+} dependent exocytosis, membrane trafficking, von-Willebrand factor

Abstract

Endothelial cells respond to blood vessel injury by the acute release of pro-coagulant von-Willebrand factor (VWF) that is stored in unique secretory granules called

Weibel-Palade bodies (WPBs). Stimulated WPB exocytosis critically depends on the proper recruitment of WPBs to the plasma membrane but factors involved in WPB-plasma membrane tethering are not known. Here we identify Munc13-4, a protein mutated in familial hemophagocytic lymphohistiocytosis 3 (FHL3), as a WPB tethering factor. Munc13-4 promotes histamine-evoked WPB exocytosis, it is present on WPBs, and secretagogue stimulation triggers an increased recruitment of Munc13-4 to WPBs and a clustering of Munc13-4 at sites of WPB-plasma membrane contact. We also identify the S100A10 subunit of the annexin A2 (AnxA2)-S100A10 protein complex as a novel Munc13-4 interactor and show that AnxA2-S100A10 participates in recruiting Munc13-4 to WPB fusion sites. These findings indicate that Munc13-4 supports acute WPB exocytosis by tethering WPBs to the plasma membrane via AnxA2-S100A10.

Introduction

Weibel-Palade bodies (WPBs) are unique secretory organelles of endothelial cells that serve as storage granules for important regulators of vascular homeostasis. Factors that are stored in WPBs for acute release on demand include the coagulant glycoprotein von-Willebrand factor (VWF) and the leukocyte receptor P-selectin (for review see (Sadler, 1998; Wagner and Frenette, 2008)). WPBs have an elongated shape that is dictated by the tight packaging of their major cargo, VWF. They form at the trans-Golgi network and are then transported along microtubules towards the cell periphery where they are anchored at the actin cytoskeleton for final maturation (for review see (Nightingale and Cutler, 2013; Valentijn and Eikenboom, 2013)). Exocytosis of the fully matured WPBs is evoked by a varied set of secretagogues such as histamine and thrombin that function by eliciting intracellular Ca^{2+}-signals, or epinephrin and vasopressin that elevate intracellular cAMP (for review see (Datta and Ewenstein, 2001; Nightingale and Cutler, 2013)). Typically, acute WPB secretion is initiated following blood vessel injury or local inflammatory activation. It results in a marked change of endothelial surface properties, rapidly transforming the anti-adhesive surface of resting endothelial cells, which supports the unrestricted circulation of blood cells, to an adhesive one capable of capturing platelets and leukocytes. Thus, controlled WPB exocytosis serves an important role in regulating blood vessel homeostasis.

Several factors involved in WPB maturation and exocytosis have been described. They include the Rab GTPases Rab3, Rab15 and Rab27a and some of their effectors (Knop *et al.*, 2004; Nightingale *et al.*, 2009; Bierings *et al.*, 2012; van Hooren *et al.*, 2012; Zografou *et al.*, 2012). Rab27a is of particular interest as it is a specific marker for mature WPBs and is also found on other lysosome-related organelles such as melanosomes that share certain properties with WPBs (for review see (Marks *et al.*, 2013)). Rab27a is involved in anchoring maturing WPBs at the cortical actin cytoskeleton via a tripartite complex consisting of Rab27a, the Rab27a effector MyRIP and myosin Va (Nightingale *et al.*, 2009; Rojo Pulido *et al.*, 2011b; Conte *et al.*, 2016). However, Rab27a has also been shown to serve as a positive regulator of stimulated WPB secretion, in this case exerting its role via another effector, the synaptotagmin-like protein Slp4a (Bierings *et al.*, 2012). Thus, Rab27a appears to fulfill several functions in WPB exocytosis with its activity being controlled by interaction with MyRIP and Slp4a, respectively, and possibly other effectors not yet identified.

Once WPBs are committed to exocytosis, the actual fusion reaction is mediated by one or several different SNARE complexes. WPB-associated VAMP3 and plasma membrane-localized syntaxin-4 and SNAP-23 form a trans-SNARE complex that mediates Ca^{2+}-evoked WPB exocytosis and possibly functions in conjunction with accessory proteins such as StxBP1 and StxBP5 (Munc18-1 and -5) (Matsushita *et al.*, 2003; Rojo Pulido *et al.*, 2011a; van Breevoort *et al.*, 2012; Breevoort *et al.*, 2014). However, it is unknown how the cortically anchored WPBs are transferred to the fusion-mediating SNARE machinery following secretagogue stimulation and whether a plasma membrane-tethered WPB intermediate is formed in the course of acute WPB exocytosis.

To identify endothelial cell components involved in a plasma membrane tethering of WPBs, we focused on Munc13 proteins that are thought to function as tethering/priming factors in other Ca^{2+}-dependent exocytotic events (for review see (James and Martin, 2013)). We show here that two Munc13 isoforms, Munc13-2 and Munc13-4 are expressed in endothelial cells. One of them, the Rab27a effector Munc13-4 localizes to WPBs and stimulates WPB exocytosis, however

independently of its interaction with Rab27a. Histamine stimulation triggers a clustering of Munc13-4 at sites of WPB-plasma membrane contact that is mediated by the terminal C2 domains of the protein. In search of novel interactors of these C2 domains we identify the S100A10 subunit of the AnxA2-S100A10 complex. AnxA2-S100A10 is recruited to the endothelial plasma membrane following histamine stimulation and participates in the formation and/or stabilization of Munc13-4 clusters at WPB fusion sites. Our data indicate that Munc13-4 tethers fusion-competent WPBs at the plasma membrane via an interaction with the S100A10 subunit of plasma membrane-bound AnxA2-S100A10 complexes.

Results

Munc13-4 is recruited to WPBs in a Rab27a-independent manner

To probe for the expression of different Munc13 isoforms in primary human endothelial cells (HUVEC), we carried out a comprehensive Western blot screen using a panel of Munc13 antibodies. In these experiments, mouse brain and lung lysates from wild-type and Munc13 knock-out mice served as positive and negative controls for antibody specificity. The blots revealed that Munc13-2 and Munc13-4 show significant expression, whereas Munc13-1 and Munc13-3 are expressed at very low levels or not at all (Fig. 1a-d). These findings were corroborated by RT-PCR analysis (Fig. 1e) and are in line with a previous report on the expression of Munc13-4 in HUVEC (Zografou *et al.*, 2012).

In our next experiments we concentrated on Munc13-4 that had been implicated in other regulated exocytosis events in non-neuronal cells, including the ATP/VEGF/bFGF-triggered release of VWF from endothelial cells (Zografou *et al.*, 2012; James and Martin, 2013). We first established by immunofluorescence staining that endogenous Munc13-4 is present on WPBs (Fig. 1f). Different fluorescent protein (FP)-tagged Munc13-4 constructs (GFP or YFP) showed the same WPB localization (Fig. 2) and were then used to record the distribution of Munc13-4 in live cells. Because some cytosolic and/or membrane fluorescence was observed in the Munc13-4 staining, the contribution of plasma membrane-associated Munc13-4 to this staining was analyzed directly by employing total internal reflection fluorescence (TIRF) microscopy, which only records signals from fluorophores excited within 100

to 200 nm of the plasma membrane at the glass interface. This revealed that Munc13-4, in addition to localizing to peripheral WPBs residing in the TIRF field, also showed some general colocalization with the plasma membrane marker PLC-PHD, encoding the PI(4,5)P_2-binding domain of phospholipase Cδ (Fig. 2b). As Munc13-4 is a known Rab27a effector and Rab27a is highly enriched on WPBs, we analyzed whether Rab27a recruits Munc13-4 to WPBs. To this end, we recorded the localization of a Munc13-4 mutant lacking the Rab27a binding motif, which had been previously identified to encompass residues 280-285 (Elstak *et al.*, 2011). Interestingly, this Munc13-4(Δ280-285) mutant still localized to WPBs, indicating that Rab27a is not required for the WPB association of Munc13-4 (Fig. 2c). This was corroborated by knockdown experiments revealing that depletion of Rab27a has no effect on the WPB localization of Munc13-4 (Fig. 2d; see Fig. S1a for Rab27a knockdown). WPBs in Rab27a-depleted cells show a less peripheral and more perinuclear distribution. This has been reported before and is caused by loss of peripheral anchorage at the cortical cytoskeleton mediated by the Rab27a/MyRIP/moysinVa complex (Nightingale *et al.*, 2009; Rojo Pulido *et al.*, 2011b). When quantified, Munc13-4 colocalized with at least 75% of all WPBs of a cell, regardless of whether Rab27a was present or not. Similarly, the Rab27a binding-deficient mutant Munc13-4(Δ280-285) also colocalized with about 75% of all cellular WPBs (Fig. S1b).

To identify sequences in Munc13-4 that mediate WPB association, we next employed a series of other mutant Munc13-4 constructs and recorded their distribution in HUVEC (for schematic illustrations of the domain structure of Munc13-4, see Fig. 3). These analyses revealed that the terminal C2 domains are dispensable but that sequences in the Munc homology domains (MHD) 1 and 2 are essential for WPB association of Munc13-4 (Fig. 3; Fig. S2 for quantification of the colocalization). Thus, while Rab27a does not participate in targeting Munc13-4 to WPBs, the MHD1/2 region is of critical importance for mediating the WPB association of Munc13-4, possibly by binding to a still unknown receptor on WPBs.

Munc13-4 supports histamine-induced WPB exocytosis independently of Rab27a

Munc13-4 is associated with WPBs and is involved in other regulated secretory events, e.g. the Ca^{2+}-stimulated exocytosis of dense-core granules in mast cells (Neeft *et al.*, 2005) and the ATP/VEGF/bFGF-triggered release of VWF from endothelial cells (Zografou *et al.*, 2012). Thus, we next analyzed whether Munc13-4 is functionally involved in histamine-evoked and Ca^{2+}-dependent WPB exocytosis in HUVEC. For this purpose, we depleted endogenous Munc13-4 by siRNA (Fig. 4a) and assessed the effect on histamine-stimulated WPB exocytosis by quantifying the amount of VWF released into the cell culture supernatant. While knockdown of Munc13-4 had no significant effect on total cellular VWF levels (Fig. S3) and basal VWF secretion, it significantly reduced the histamine-triggered release of VWF (Fig. 4b). To verify the specificity of the knockdown effect, we generated a siRNA-insensitive wildtype YFP-Munc13-4 construct that was expressed in siRNA-transfected cells. This construct fully restored histamine-evoked VWF secretion, confirming that Munc13-4 functions as a positive regulator in Ca^{2+}-dependent WPB exocytosis. We then assessed whether an interaction with Rab27a is required for the activity of Munc13-4 in WPB exocytosis. Therefore, we expressed in the siRNA-treated cells a siRNA-insensitive version of the Munc13-4(Δ280-285) mutant deficient in binding Rab27a. This mutant also efficiently restored histamine-evoked secretion in Munc13-4-depleted cells (Fig. 4b). Thus, Munc13-4 is a positive regulator of Ca^{2+}-dependent WPB exocytosis and this function does not depend on Rab27a binding.

Munc13-4 is recruited to membrane-associated WPBs following secretagogue stimulation

We next analyzed whether the intracellular distribution of Munc13-4 is affected by secretagogue stimulation of HUVEC and recorded the dynamic localization of FP-tagged Munc13-4 constructs in histamine-stimulated HUVEC by live confocal and TIRF microscopy. A quantitative analysis of the respective fluorescence images revealed that histamine triggers an increase of Munc13-4 at WPBs, including those residing in the cell periphery (Fig. 5a). To relate the stimulation-induced enrichment of Munc13-4 at peripheral, possibly plasma membrane-tethered WPBs to the actual sites of WPB docking and fusion, we coexpressed YFP-Munc13-4 with VWF-RFP, which served as a WPB marker. Sites of WPB exocytosis can thus be easily

identified by a collapse of the VWF-RFP-labelled rod-like WPB structure into a round spot that can be recorded with high spatial and temporal resolution by TIRF microscopy. Analyses of fusing WPBs revealed that the YFP-Munc13-4 fluorescence, after an initial increase at the WPB before fusion, rapidly disappears after fusion, i.e. when the elongated VWF-RFP-positive WPB structure collapses into a bright fusion spot (Fig. 5b, c; Suppl. video Fig5video01). Externalized VWF-RFP, on the other hand, remains present as a round spot at the fusion site for a considerable length of time, probably because large VWF multimers are trapped at the extracellular matrix on the coverslip.

Next, live-cell TIRF microscopy was employed to analyze whether histamine stimulation also affects the distribution of YFP-Munc13-4 at the plasma membrane prior to or at the time of the fusion event. Figure 6a shows that the relatively homogeneous plasma membrane signal of Munc13-4, which is seen in addition to the WPB staining in resting cells (see also Fig. 2b), becomes concentrated in more distinct foci following histamine treatment. In many cases, these foci colocalized with VWF-RFP-labelled WPBs that were detectable in the TIRF field and eventually underwent fusion (Fig. 6a; Suppl. Video Fig6video02). To better describe the dynamic nature of the FP-Munc13-4 foci, TIRF recordings were analyzed using an object detection algorithm that identifies bright objects of a size range covering the dimensions of WPBs (MorphoQuant, see Methods for details (Schuberth *et al.*, 2015)). The number of Munc13-4-positive objects most likely reflecting Munc13-4 foci tethering WPBs at the plasma membrane increased sharply following histamine stimulation and then decreased again with slower kinetics (Fig. 6b). The decrease most likely results from a loss of Munc13-4 from sites of WPB fusion and the diffusion of Munc13-4 in the membrane (see also Fig. 5b, c). It should be noted that not all YFP-Munc13-4-positive foci colocalized with VWF-RFP-labelled WPBs. A considerable number appeared at sites where no VWF-RFP signal was visible in the TIRF field. These might represent tethering sites of older WPBs not labelled with the transiently expressed VWF-RFP; they might reflect a transient enrichment of Munc13-4 at docking sites of other secretory vesicles; and/or they might have arisen from an intrinsic Ca^{2+}-induced clustering of membrane-associated Munc13-4.

As the data described above indicate a role of Munc13-4 in tethering fusion-competent WPBs at the plasma membrane, we next employed the object detection algorithm together with the expression of Munc13-4 mutants to analyze which Munc13-4 domains are required for foci formation at the plasma membrane. These experiments revealed that both terminal C2 domains are indispensable for this foci formation. Truncations of the C2 domains as well as point mutations affecting Ca^{2+} binding (Boswell *et al.*, 2012) largely abolished the histamine-triggered formation of Munc13-4 foci (Fig. 7). As expected from our previous analyses, Rab27a binding was not required for foci formation because the characteristic transient foci were also observed for the Munc13-4(Δ280-285) mutant (Fig. 7). Together the experiments with mutant Munc13-4 variants indicate that the central MUN domain of Munc13-4 targets the protein to WPBs, whereas following histamine stimulation, the C2A and C2B domains are required for inducing an enrichment of Munc13-4 at WPB-plasma membrane fusion sites prior to fusion.

Exocytosis of WPBs can also be induced by cAMP-elevating agents such as forskolin, although some differences appear to exist between the Ca^{2+}- and cAMP-dependent pathways (for review see (Datta and Ewenstein, 2001; Nightingale and Cutler, 2013)). Therefore, we analyzed whether the transient Munc13-4 foci can also be elicited by forskolin. Interestingly, this was not the case (Fig. S4).

Munc13-4 interacts with the S100A10 subunit of the AnxA2-S100A10 complex

Given the importance of the C2 domains of Munc13-4 in directing the protein to plasma membrane sites where WPB fusions occur, we performed a yeast two-hybrid (YTH) screen with the two C2 domains of Munc13-4 as baits. The predominant potential interaction partner identified in this screen was S100A10; 42 of the 71 positive clones obtained in the screen with the C-terminal C2 domain contained the complete coding sequence of S100A10 (see Suppl. Information for details). S100A10 is a member of the EF-hand superfamily of Ca^{2+}-binding proteins (Fig. 8a). It resides in a tight heterotetrameric complex with AnxA2, a Ca^{2+}-regulated phospholipid and plasma membrane binding protein, and the complex acts as a positive regulator of acute WPB exocytosis by a yet unknown mechanism (Knop *et al.*, 2004; Brandherm *et al.*, 2013). To confirm the interaction of Munc13-4 with S100A10 and to map their respective binding sites, we performed pull-down experiments with recombinantly

expressed and purified Munc13-4 and S100A10 derivatives. This revealed that S100A10 and Munc13-4 directly interact with one another and that both C2 domains of Munc13-4 bind S100A10 (Fig. 8b). We also obtained quantitative binding parameters by surface plasmon resonance (K_D=0.45 μM, Fig. S5). Pull-down experiments with different S100A10 mutants revealed that in S100A10 the binding site for Munc13-4 resides in the very C-terminal six residues (amino acid 91-96) (Fig. 8c). This region is dispensable for AnxA2 binding (Kube *et al.*, 1992), indicating that S100A10 can bind simultaneously to AnxA2 and Munc13-4. To test whether tripartite AnxA2/S100A10/Munc13-4 complexes do form in endothelial cells, we carried out co-immunoprecipitation (co-IP) experiments. These revealed a significant co-IP of all three proteins from HUVEC lysates in the absence of Ca^{2+} (Fig. 8d; quantification of co-IP results for Munc13-4 and S100A10 in Fig. 8e). Thus, tripartite complexes of S100A10 binding both AnxA2 and Munc13-4 do form in HUVEC and Munc13-4 is recruited to these complexes via its C2 domains.

Given the likely tethering function of Munc13-4 in WPB exocytosis, we also assessed whether AnxA2-S100A10 participates in a Munc13-4-mediated tethering of WPBs. A prerequisite for such a function would be a histamine-evoked and thus Ca^{2+}-induced recruitment of AnxA2-S100A10 to the plasma membrane because the majority of AnxA2-S100A10 resides in the cytoplasm of non-stimulated HUVEC (Knop *et al.*, 2004). As revealed by live-cell TIRF microscopy, histamine stimulation leads to a marked increase of FP-tagged AnxA2 and S100A10 at the plasma membrane, most likely due to a membrane translocation from the cytosol (Fig. S6a, b; see also Suppl. videos FigS6video03 and FigS6video04). Some of the translocated S100A10 also becomes enriched at the stimulation-induced Munc13-4 foci that occur at sites of WPB tethering and fusion (Fig. S6c; see also Suppl. video FigS6video05).

Next, we analyzed a potential role of AnxA2-S100A10 in the formation and/or stabilization of the Munc13-4 tethers. Therefore, we depleted HUVEC of AnxA2 and S100A10 by siRNA knockdown and determined the level of Munc13-4 at WPB docking/fusion sites by recording histamine-induced changes in Munc13-4-mKate fluorescence in live HUVEC using TIRF microscopy. As expected, control siRNA-transfected cells show a histamine-triggered increase of WPB-associated Munc13-4-mKate fluorescence that decreases after fusion (Fig. 9a). This transient increase is

markedly reduced following AnxA2-S100A10 knockdown (Fig. 9a, b) indicative of a function of AnxA2-S100A10 in recruiting Munc13-4 to WPB-plasma membrane contact sites or stabilizing Munc13-4 clusters at these sites.

Finally, we determined whether the interaction of Munc13-4 with AnxA2-S100A10 is functionally relevant for WPB exocytosis. Therefore, HUVEC were depleted of Munc13-4 or S100A10, or of Munc13-4 plus S100A10 in a double knockdown approach. We then assessed the effects on histamine-evoked WPB exocytosis by quantifying the amount of secreted VWF. The results confirmed the reduction of histamine-stimulated VWF secretion by Munc13-4 (see Fig. 4) or S100A10 depletion (Knop *et al.*, 2004). Importantly, the simultaneous knockdown of Munc13-4 and S100A10 had no additional inhibitory effect (Fig. 9c; see Fig. S7 for knockdown efficiency). This suggests that the proteins function in a common pathway and supports the notion that a tripartite Munc13-4/S100A10/AnxA2 complex is a positive regulator of WPB exocytosis.

Discussion

WPBs are secretory organelles of vascular endothelial cells that serve an important role in controlling blood vessel homeostasis. WPB exocytosis exposes the adhesive platelet and leukocyte receptors VWF and P-selectin, thereby rapidly converting the anti-adhesive endothelial surface to an adhesive one, for example after blood vessel injury or local inflammatory activation. Hence, the exocytosis of WPBs has to be strictly regulated and can be evoked by secretagogue stimulation and the subsequent transient increase in intracellular Ca^{2+}. Although this Ca^{2+}-dependent WBP exocytosis is well documented, the Ca^{2+}-sensors and tethering/priming factors involved are not known. Here, we identify a novel complex consisting of Munc13-4 and AnxA2-S100A10 as a positive regulator of Ca^{2+}-evoked WPB exocytosis. Munc13-4 is present on WPBs in resting endothelial cells and clusters at sites of WPB exocytosis following histamine stimulation. It interacts directly with the S100A10 subunit of the AnxA2-S100A10 complex, which is recruited to the plasma membrane following secretagogue stimulation and facilitates Munc13-4 clustering, and both, Munc13-4 and AnxA2-S100A10 are required for efficient histamine-stimulated WPB exocytosis.

Munc13-4 functions in regulated exocytosis in different non-neuronal cells, often of hematopoietic origin, including mast cells, endothelial cells stimulated with a mixture of ATP/VEGF/bFGF and cytotoxic T lymphocytes (Feldmann *et al.*, 2003; Neeft *et al.*, 2005; Zografou *et al.*, 2012). It has been suggested that the protein acts as a tethering and priming factor in granule-plasma membrane interactions, although direct evidence for these tethers is still lacking (James and Martin, 2013). Our data are in line with a tethering function of Munc13-4 and provide evidence for the existence of tethering complexes in endothelial cells as we see an increased FP-Munc13-4 signal in distinct plasma membrane foci that are induced by secretagogue stimulation and coincide with WPB fusion sites. In resting HUVEC, Munc13-4 is found on WPBs although a fraction of the protein also resides at the plasma membrane and in the cytosol. Histamine stimulation triggers a transient increase at and redistribution of Munc13-4 to the foci that most likely represent WPB tethering complexes. This redistribution requires the terminal C2 domains, indicating that Ca^{2+}-binding and/or specific protein or lipid interactions of these C2 domains are relevant for the tethering function. As the C2A domain can interact with different syntaxins and the C2B domain can bind certain phospholipids (Boswell *et al.*, 2012), these interactions, induced by secretagogue-stimulated Ca^{2+}-increase, could trigger or assist the enrichment of Munc13-4 at WPB fusion sites. Such interactions are likely to occur after complex formation of Munc13-4 with AnxA2-S100A10 following a Ca^{2+}-dependent translocation of AnxA2-S100A10 to the plasma membrane. In this scenario, subsequent SNARE interactions of plasma membrane-docked Munc13-4 could help stabilize the tether and could also initiate a priming of tethered WPBs leading to SNARE-mediated fusion. A function of Munc13-4 in linking tethered WPBs to the SNARE fusion machinery is in line with the finding that the C2A domain binds syntaxins 2 and 4, which both have been implicated in WPB exocytosis (Matsushita *et al.*, 2003; Rojo Pulido *et al.*, 2011a; Boswell *et al.*, 2012).

We show here that histamine stimulation promotes a translocation of cytoplasmic AnxA2-S100A10 to the plasma membrane, most likely by inducing Ca^{2+}-dependent phospholipid binding in the AnxA2 subunits (Fig. S6). In the resulting membrane-bound conformation of AnxA2-S100A10, the two AnxA2 subunits likely face the membrane through direct interaction with acidic phospholipids, such as PA, $PI(4,5)P_2$ and/or PS, whereas the S100A10 subunits point towards the cytosol (Menke *et al.*,

2005). The S100A10 subunit is then available for additional interactions, and thereby the entire complex can serve as a Ca^{2+}-regulated plasma membrane targeting module for S100A10 binding proteins. A number of such proteins have been described, e.g. the Ca^{2+}-channels TRPV5 and TRPV6, the sodium channel Nav1.6 and the serotonin 5-HT1B receptor (Okuse *et al.*, 2002; van de Graaf *et al.*, 2003; Svenningsson *et al.*, 2006). Here we identify Munc13-4 as a new S100A10 interaction partner that can use the AnxA2-S100A10 module as a means to trigger and/or stabilize a plasma membrane-bound state required for efficient tethering of WPBs (see Fig. 9a, b). In this scenario, AnxA2-S100A10 regulates Munc13-4-mediated tethering, and this function, in turn, is regulated by Ca^{2+}-triggered membrane targeting of the AnxA2-S100A10 complex itself.

In other secretory cell types, Munc13-4 function depends on a Rab27a-mediated association with secretory granules that are often considered lysosome-related (James and Martin, 2013). However and in contrast to secretory events involving other lysosome-related organelles, a Rab27a-Munc13-4 interaction is required neither for recruiting Munc13-4 to WPBs nor for Munc13-4 to promote WPB exocytosis (Fig. 2 and 4). Rather, we identified a sequence towards the C-terminal end of the central MUN domain that is indispensable for WPB interaction. The different domains in Munc13-4 therefore integrate several interactions crucial for efficient WPB exocytosis: (1) A MUN domain-mediated anchoring of Munc13-4 to WPBs; (2) a C2 domain-mediated link to AnxA2-S100A10 at the plasma membrane; (3) an interaction of Munc13-4 with both syntaxins and certain lipids mediated by its C2A and C2B domains, respectively. Thus, the mechanism underlying Munc13-4 function in endothelial cells appears to be unique as it does not involve an interaction with Rab27a. Interestingly, FHL3 patients who carry mutations in Munc13-4 show no overt bleeding phenotype, i.e. no severe compromise in VWF secretion. This lack of a severe bleeding phenotype is possibly due to the unperturbed cAMP-dependent WPB exocytosis (see Fig. S6). Future analysis of FHL3 patients might reveal more subtle or acute bleeding phenotypes due to altered Munc13-4 activity in endothelial cells.

Materials and methods

Antibodies, plasmids, siRNA, reverse transcriptase-PCR and surface plasmon resonance

The experimental details are described in Supplementary Information.

HUVEC culture and transfection

Primary human umbilical vein endothelial cells (HUVEC) were either isolated from umbilical cord veins as described before (Jaffe *et al.*, 1973) and used as fresh or cryoconserved preparations, or purchased as cryoconserved pools (Promocell). Cells were maintained in mixed endothelial growth medium (ECGM1, Promocell, mixed 1:1 with M199, Biochrom, supplemented with 10% FCS, 20 µg/ml gentamycin, 15 µg/ml amphotericin B and 100 I.E. Heparin) or endothelial growth medium (ECGM2, Promocell; supplemented with 20 µg/ml gentamycin, 15 µg/ml amphotericin B), and cultured and transfected as described before (Knop *et al.*, 2004). Nearly confluent cells at passages 2-4 were used in all experiments.

Western blot

For the Western blot detection of Munc13 isoforms in HUVEC, we employed as controls postnuclear supernatants from mouse brains or lungs that were prepared by homogenization in lysis buffer (320 mM sucrose, 2 mM EDTA, 20 mM HEPES/NaOH to pH 7.4) and centrifugation (1000 g for 10 min at 4°C). HUVEC lysates were prepared as total lysates by washing a 60 mm plate once with PBS on ice, scratching the cells into 40 µl sample buffer (6% (w/v) SDS, 150 mM Tris/HCl pH 6.8, 30% (v/v) glycerol, 0.01% (w/v) bromophenol blue, 10% (w/v) DTT) and boiling at 95°C for 10 min. Samples were subjected to SDS-PAGE in 8% acrylamide gels, transferred to a nitrocellulose membrane at 50 mA overnight in Tris-glycine buffer (25 mM Tris, 190 mM glycine, 20% (v/v) methanol) and blocked for 1 h in TBS containing 0.1% Tween-20 (TBS-T), 5% milk powder and 5% goat serum. Membranes were incubated with the respective primary antibodies overnight and subsequently with the HRP- or IR-coupled secondary antibodies for 1 h, with extensive washings (TBS-T with 5% milk powder) after each antibody incubation. Signals were detected by chemiluminescence or using the Odyssey Infrared Imaging System (LI-COR). For Western blot detection of S100A10 and AnxA2, we employed standard procedures and 10% or 15% SDS-PAGs.

VWF secretion assay

HUVEC were stimulated with 100 μM histamine (Sigma-Aldrich) or 1 μM ionomycin and the amount of secreted VWF was quantified by ELISA as described before (Rojo Pulido *et al.*, 2011b), analyzing three triplicate samples per condition (supernatant of unstimulated cells, of stimulated cells, and total lysates). The amount of VWF secreted into the cell culture supernatant was then expressed as percentage of total VWF content (amount of VWF of all three samples summed up, i.e. supernatant of non-stimulated plus supernatant of stimulated cells plus remaining total lysate). This analysis allowed to control for differences in total VWF content between each replicate and each condition.

Yeast two-hybrid screening

Bait vectors encoding the LexA DNA binding domain in frame with rat Munc13-4 (GenBank accession number AF159356 (Koch *et al.*, 2000); residues 1-303 (N-terminal C2) or 888-1088 (C-terminal C2) were constructed in pLexN (Vojtek *et al.*, 1993; Betz *et al.*, 1997). Yeast two-hybrid screens using a rat lung cDNA MATCHMAKER prey library in pACT2 (Clontech) were performed as described (Fields and Song, 1989; Betz *et al.*, 1997).

The YTH screen with the N-terminal C2 domain of Munc13-4 yielded 78 positive clones from 31 million double transformants. Of these, 37 encoded the full-length cardiac Troponin 1 (Tnni3), and 18 encoded the $GABA_A$-receptor associated protein Gabarap. All 18 Gabarap clones encoded the complete C-terminus of the protein, but lacked the codons for the first 10 (11 clones) or 43 N-terminal residues (7 clones). Less frequently isolated positive prey clones (each <5 % of the total) encoded fragments of Rgs3, Ulc1, Ndn, and Rps18. The YTH screen with the C-terminal C2 domain of Munc13-4 yielded 71 positive clones from 170 million double transformants. Of these, 42 contained the complete coding sequence of S100A10, and 12 encoded the complete coding sequence of Sorting Nexin 5 (Snx5). Less frequently isolated positive prey clones (each <5 % of the total) encoded fragments of Naa10, Scgb1a1, Tdrd7, Eif1a, and Rps18.

Co-immunoprecipitation

For the immunoprecipitation of Munc13-4, we employed rabbit polyclonal anti-Munc13-4 (Proteintech or SantaCruz, sc-50465) and, as control, non-specific rabbit IgGs that were coupled to anti-rabbit IgG Dynabeads (Invitrogen) or Protein A-Agarose beads (SantaCruz). HUVEC were washed twice with ice-cold PBS, harvested with a cell scraper and collected by low speed centrifugation. The cell pellets were resuspended in ice-cold lysis buffer (20 mM HEPES pH 7.4, 150 mM NaCl, 0.5% NP-40, Complete EDTA-free Protease Inhibitor Cocktail, Roche), lysed by passage through a 23 gauge needle and post nuclear supernatants (PNS) were prepared by centrifugation of the lysates (1,000 x g, 10 min, 4°C). Immunoprecipitations were carried out by incubating the PNS with the respective beads for 2 h or 4 h at 4°C, and subsequently, the beads were washed three times with ice-cold lysis buffer or washing buffer (20 mM Hepes pH 7.4, 500 mM NaCl, 0.5% NP-40) using a magnetic particle concentrator (Invitrogen) or low speed centrifugation. After the last wash, proteins bound to the beads were released by resuspending the beads in SDS protein loading buffer [50 mM Tris–HCl pH 6.8, 2% (w/v) SDS, 10% (v/v) β-mercaptoethanol, 10% (v/v) glycerol, 0.1% (w/v) Bromophenol blue], and analyzed by Western blotting with rabbit and goat polyclonal anti-Munc13-4 antibodies, anti-S100A10 and anti-AnxA2 antibodies, and with IR-dye coupled secondary antibodies as described above (Western blot).

Expression of His_6-tagged Munc13-4 derivatives

His_6-tagged derivatives of Munc13-4 were expressed in *E. coli* (BL21) following overnight induction with 0.1 mM IPTG at 25°C to reduce protein misfolding and degradation. Bacteria were harvested by centrifugation and resuspended in lysis buffer (40 mM HEPES pH 7.5, 20 mM imidazole, 300 mM NaCl, 1 mM EDTA, 10 mM 2-Mercaptoethanol, Complete EDTA-free Protease Inhibitor Cocktail, Roche). Cell lysis was achieved by four freeze/thaw cycles and six 1 min sonication steps, and soluble lysates containing His_6-tagged Munc13-4 were obtained by ultracentrifugation (100,000 x g, 1 h, 4°C).

Expression and purification of untagged S100A10

Bacterial expression of S100A10 followed a similar protocol as the one used for His_6-tagged derivatives of Munc13-4 (see above), but treatment with 1 mM IPTG for 4 h at

37°C was used for induction of recombinant protein expression, and a modified lysis buffer was employed (200 mM Tris/HCl pH 7.5, 200 mM NaCl, 10 mM $MgCl_2$, 1 mM NaN_3, 2 mM DTT, Complete EDTA-free Protease Inhibitor Cocktail). Different protocols were then employed to prepare wild-type S100A10 or the truncated S100A10 mutants (residues 1-90, 1-84). Wild-type S100A10 was purified from the soluble bacterial lysate by ion exchange chromatography in two consecutive steps (modified after (Kube *et al.*, 1992)) using the weak anion exchanger DEAE sephacel (Diethylaminoethyl, GE Healthcare; DEAE buffer, 20 mM imidazole pH 7.5, 50 mM NaCl, 2 mM DTT, 5 mM EDTA, 0.5 mM EGTA, 1 mM NaN_3), and applying the flow-through to the weak cation exchanger CM52 cellulose (carboxymethyl, Whatman; CM buffer 20 mM sodium acetate pH 5.6, 2 mM DTT, 0.5 mM EDTA, 0.5 mM EGTA, 1 mM NaN_3). After extensive washing with CM buffer and CM buffer containing 100 mM NaCl, wild-type S100A10 was eluted with 500 mM NaCl in CM buffer. S100A10(1-90) and S100A10(1-84) could not be eluted from the CM matrix material and were purified using a different protocol(Ayala-Sanmartin *et al.*, 2000). Briefly, cleared bacterial lysates were first subjected to $(NH_4)_2SO_4$ precipitation at 50% saturation. After centrifugation (50,000 x g, 30 min), the non-precipitated fraction was applied to a phenyl sepharose matrix (GE Healthcare) that retained the S100A10 derivatives. The matrix was washed with loading buffer and bound proteins were eluted with decreasing concentrations of $(NH_4)_2SO_4$ in lysis buffer (50%, 25%, 15% and 0% saturation of $(NH_4)_2SO_4$). The last two fractions containing the S100A10 derivatives were applied to DEAE sephacel equilibrated in DEAE buffer. The column was washed with DEAE buffer containing 100 mM NaCl and proteins were eluted with 300 mM NaCl in DEAE buffer.

In vitro binding assay with His_6-Munc13-4 variants and S100A10

Soluble fractions of His_6-Munc13-4 or cleared lysates of untransformed BL21 bacteria as control were incubated with NiNTA beads equilibrated in assay buffer (40 mM HEPES pH 7.5, 20 mM imidazole, 300 mM NaCl, 0.5 mM EDTA, 10 mM 2-mercaptoethanol, 1 mM $CaCl_2$) for 15 min at 4°C. After two washings with ten column volumes of assay buffer, equal amounts of wild-type or mutant S100A10 dialyzed against assay buffer were applied to the column. After several washings with ten column volumes of assay buffer, His_6-Munc13-4 and potentially interacting S100A10 were released with elution buffer containing 300 mM imidazole (300 mM imidazole,

300 mM NaCl, 1 mM $MgCl_2$, 10 mM 2-mercaptoethanol) in several steps. Samples of all steps were run on 15% SDS-PAGs, transferred to nitrocellulose membranes and analyzed by probing with anti-penta-Histidine and anti-S100A10 (H21) antibodies as described above (Western blot).

Confocal and TIRF microscopy

Cells were grown on collagen-coated coverslips or chambered slides (Nunc Labtek Chambered Coverglass) for 48 h after transfection if not stated otherwise. For analysis of fixed cells, samples were treated with 4% PFA (30 min, RT) or methanol (10 min, -20°C), permeabilized with 0.1% Triton-X100 (15 min, RT), and mounted in Mowiol. Live cells were imaged in medium supplemented with 25 mM HEPES at 37°C. Confocal imaging employed a Zeiss LSM780 confocal microscope and a Plan-Apochromat 63x/1.4 oil immersion objective. Confocal videos were recorded at different speeds. TIRF imaging was performed with an Olympus IX71 TIRF Microscope customized to include a heated incubation chamber, an objective-type TIRFM setup from TILL Photonics, a monochromator for epifluorescence excitation, and a controller allowing hardware-controlled fast switching between total internal reflection fluorescence and epifluorescence (TILL Photonics). Images were acquired using a TILL Image QE charge-coupled device camera (TILL Photonics) and MetaMorph Software (Molecular Devices). The total internal reflection angle was manually adjusted for every experiment. TIRF time-lapse movies were recorded with 2-5 frames per second. Image analysis was performed in ImageJ.

Stimulation-induced recruitment of Munc13-4 to WPBs

Stimulation-induced recruitment of Munc13-4 to WPBs was measured in TIRF microscopy recordings or confocal sections of cells expressing VWF-RFP or VWF-GFP and YFP-Munc13-4 or Munc13-4-mKate, respectively. Image stills were thresholded in ImageJ to create regions-of-interest (ROIs) for Munc13-4-positive WPBs in a cell and to compare mean fluorescence intensities of all ROIs before and after stimulation. ROIs were manually inspected to delete those that did not include the same WPBs in both frames because the WPBs had moved. Mean fluorescence intensities before stimulation were set as 1; the increase after stimulation was measured as the n-fold change in mean fluorescence intensities for every individual ROI. Mean n-fold changes from all individual ROIs were tested for statistical

significance by one-sample t-test from n=323 WPBs and seven independent experiments (Fig. 5) and by Mann-Whitney U test from at least n=57 WPBs per conditions and at least three independent experiments (Fig. 9b and c).

Automated object detection

Munc13-4-positive objects were detected in TIRF live recordings before and after stimulation using the Matlab-based image-processing algorithm MorphoQuant, which was originally developed to detect Golgi structures (Schuberth *et al.*, 2015). MorphoQuant is freely available at https://github.com/tischi/MorphoQuant. The algorithm detects locally bright large objects of arbitrary shape. The algorithm used a top-hat filter with a circular structural element whose radius r1 was defined to include a typical WPB (r1 = 15 pixel with 1 pixel ≈ 133 nm). This filter segmented images into a foreground image containing Munc13-4-positive objects and a background image representing the Munc13-4 at the plasma membrane. Subsequent filtering steps improved the distinction between foreground objects and background signal based on their relative fluorescence intensity, defined by an adjustable threshold t1 (t1 = 8 a.u.). The procedure identified Munc13-4-positive bright objects (adjusted by t1) of a defined size (adjusted by r1) but otherwise arbitrary shape. We visually confirmed that object detection was accurate and that objects showed the typical elongated shape of WPBs. Data were prepared in Excel to illustrate the number of Munc13-4-positive objects and fluorescence of Munc13-4 on objects or non-objects over time.

Quantification of colocalization of Munc13-4 with WPBs

The fluorescence intensities of VWF were plotted across each WPB using ImageJ. The same cross section was plotted for the Munc13-4 fluorescence channel. WPBs were counted as Munc13-4-positive if the Munc13-4 fluorescence at the WPB fluorescence intensity peak was at least 1.5 times higher than background. At least 300 WPB from at least three individual experiments were quantified for each condition.

Statistical analysis

Statistical analyses were performed with GraphPad Prism 6 as indicated in the figure legends. Significance threshold was $P<0.05$. We tested for normal distribution with the D'Agostino-Pearson omnibus test. When single datasets were not normally

distributed, we confirmed the validity of the one-way ANOVA or t-test by non-parametric Kruskal-Wallis or Mann-Whitney test. Mean values are expressed as mean±SEM. In boxplots, boxes extend from 25th to 75th percentile, whiskers extend from 10th to 90th percentile, line represents the median and dots indicate outliers.

Acknowledgments

We thank Ines Rojo Pulido for initial experiments on the S100A10-Munc13-4 interaction. This work was supported by grants from the German Research Council (DFG, GE514/6-2 and GE514/10-1 to VG), the NIH (DK025861 to TFJM) and the Dutch Cancer Society (UU2003-2958 to PvdS).

References

Ayala-Sanmartin, J., Gouache, P., and Henry, J.-P. (2000). N-Terminal Domain of Annexin 2 Regulates Ca^{2+} -Dependent Membrane Aggregation by the Core Domain: A Site Directed Mutagenesis Study. Biochemistry (Mosc.) 39, 15190–15198.

Betz, A., Okamoto, M., Benseler, F., and Brose, N. (1997). Direct interaction of the rat unc-13 homologue Munc13-1 with the N terminus of syntaxin. J. Biol. Chem. 272, 2520–2526.

Bierings, R., Hellen, N., Kiskin, N., Knipe, L., Fonseca, A.-V., Patel, B., Meli, A., Rose, M., Hannah, M. J., and Carter, T. (2012). The interplay between the Rab27A effectors Slp4-a and MyRIP controls hormone-evoked Weibel-Palade body exocytosis. Blood 120, 2757–2767.

Boswell, K. L., James, D. J., Esquibel, J. M., Bruinsma, S., Shirakawa, R., Horiuchi, H., and Martin, T. F. J. (2012). Munc13-4 reconstitutes calcium-dependent SNARE-mediated membrane fusion. J. Cell Biol. 197, 301–312.

Brandherm, I., Disse, J., Zeuschner, D., and Gerke, V. (2013). cAMP-induced secretion of endothelial von Willebrand factor is regulated by a phosphorylation/dephosphorylation switch in annexin A2. Blood 122, 1042–1051.

Van Breevoort, D. et al. (2012). Proteomic Screen Identifies IGFBP7 as a Novel Component of Endothelial Cell-Specific Weibel-Palade Bodies. J. Proteome Res. 11, 2925–2936.

Breevoort, D. van et al. (2014). STXBP1 promotes Weibel-Palade body exocytosis through its interaction with the Rab27A effector Slp4-a. Blood 123, 3185–3194.

Conte, I. L., Hellen, N., Bierings, R., Mashanov, G. I., Manneville, J.-B., Kiskin, N. I., Hannah, M. J., Molloy, J. E., and Carter, T. (2016). Interaction between MyRIP and the actin cytoskeleton regulates Weibel–Palade body trafficking and exocytosis. J Cell Sci 129, 592–603.

Cooper, B. et al. (2012). Munc13-Independent Vesicle Priming at Mouse Photoreceptor Ribbon Synapses. J. Neurosci. 32, 8040–8052.

Datta, Y. H., and Ewenstein, B. M. (2001). Regulated secretion in endothelial cells: biology and clinical implications. Thromb. Haemost. 86, 1148–1155.

Elstak, E. D. et al. (2011). The munc13-4-rab27 complex is specifically required for tethering secretory lysosomes at the plasma membrane. Blood 118, 1570–1578.

Feldmann, J. et al. (2003). Munc13-4 is essential for cytolytic granules fusion and is mutated in a form of familial hemophagocytic lymphohistiocytosis (FHL3). Cell 115, 461–473.

Fields, S., and Song, O. (1989). A novel genetic system to detect protein-protein interactions. Nature 340, 245–246.

Van de Graaf, S. F. J., Hoenderop, J. G. J., Gkika, D., Lamers, D., Prenen, J., Rescher, U., Gerke, V., Staub, O., Nilius, B., and Bindels, R. J. M. (2003). Functional expression of the epithelial Ca(2+) channels (TRPV5 and TRPV6) requires association of the S100A10-annexin 2 complex. EMBO J. 22, 1478–1487.

Van Hooren, K. W. E. M., van Agtmaal, E. L., Fernandez-Borja, M., van Mourik, J. A., Voorberg, J., and Bierings, R. (2012). The Epac-Rap1 Signaling Pathway Controls cAMP-mediated Exocytosis of Weibel-Palade Bodies in Endothelial Cells. J. Biol. Chem. 287, 24713–24720.

Jaffe, E. A., Nachman, R. L., Becker, C. G., and Minick, C. R. (1973). Culture of Human Endothelial Cells Derived from Umbilical Veins. Identification by morphologic and immunologic criteria. J. Clin. Invest. 52, 2745–2756.

James, D. J., and Martin, T. F. J. (2013). CAPS and Munc13: CATCHRs that SNARE Vesicles. Front. Endocrinol. 4.

Knop, M., Aareskjold, E., Bode, G., and Gerke, V. (2004). Rab3D and annexin A2 play a role in regulated secretion of vWF, but not tPA, from endothelial cells. EMBO J. 23, 2982–2992.

Koch, H., HOFMANN, K., and Brose, N. (2000). Definition of Munc13-homology-domains and characterization of a novel ubiquitously expressed Munc13 isoform. Biochem J 349, 247–253.

Kube, E., Becker, T., Weber, K., and Gerke, V. (1992). Protein-protein interaction studied by site-directed mutagenesis. Characterization of the annexin II-binding site on p11, a member of the S100 protein family. J. Biol. Chem. 267, 14175–14182.

Marks, M. S., Heijnen, H. F. G., and Raposo, G. (2013). Lysosome-related organelles: unusual compartments become mainstream. Curr. Opin. Cell Biol. 25, 495–505.

Matsushita, K. et al. (2003). Nitric oxide regulates exocytosis by S-nitrosylation of N-ethylmaleimide-sensitive factor. Cell 115, 139–150.

Menke, M., Gerke, V., and Steinem, C. (2005). Phosphatidylserine Membrane Domain Clustering Induced by Annexin A2/S100A10 Heterotetramer. Biochemistry (Mosc.) 44, 15296–15303.

Neeft, M. et al. (2005). Munc13-4 is an effector of rab27a and controls secretion of lysosomes in hematopoietic cells. Mol. Biol. Cell 16, 731–741.

Nightingale, T., and Cutler, D. (2013). The secretion of von Willebrand factor from endothelial cells; an increasingly complicated story. J. Thromb. Haemost. 11, 192–201.

Nightingale, T. D., Pattni, K., Hume, A. N., Seabra, M. C., and Cutler, D. F. (2009). Rab27a and MyRIP regulate the amount and multimeric state of VWF released from endothelial cells. Blood 113, 5010–5018.

Okuse, K., Malik-Hall, M., Baker, M. D., Poon, W.-Y. L., Kong, H., Chao, M. V., and Wood, J. N. (2002). Annexin II light chain regulates sensory neuron-specific sodium channel expression. Nature 417, 653–656.

Rojo Pulido, I., Jahn, R., and Gerke, V. (2011a). VAMP3 is associated with endothelial Weibel–Palade bodies and participates in their Ca2+-dependent exocytosis. Biochim. Biophys. Acta BBA - Mol. Cell Res. 1813, 1038–1044.

Rojo Pulido, I., Nightingale, T. D., Darchen, F., Seabra, M. C., Cutler, D. F., and Gerke, V. (2011b). Myosin Va Acts in Concert with Rab27a and MyRIP to Regulate Acute Von-Willebrand Factor Release from Endothelial Cells. Traffic 12, 1371–1382.

Sadler, J. E. (1998). Biochemistry and Genetics of Von Willebrand Factor. Annu. Rev. Biochem. 67, 395–424.

Schuberth, C. E., Tängemo, C., Coneva, C., Tischer, C., and Pepperkok, R. (2015). Self-organization of core Golgi material is independent of COPII-mediated endoplasmic reticulum export. J. Cell Sci. 128, 1279–1293.

Svenningsson, P., Chergui, K., Rachleff, I., Flajolet, M., Zhang, X., El Yacoubi, M., Vaugeois, J.-M., Nomikos, G. G., and Greengard, P. (2006). Alterations in 5-HT1B receptor function by p11 in depression-like states. Science 311, 77–80.

Valentijn, K. M., and Eikenboom, J. (2013). Weibel-Palade bodies: a window to von Willebrand disease. J. Thromb. Haemost. JTH 11, 581–592.

Varoqueaux, F., Sons, M. S., Plomp, J. J., and Brose, N. (2005). Aberrant Morphology and Residual Transmitter Release at the Munc13-Deficient Mouse Neuromuscular Synapse. Mol. Cell. Biol. 25, 5973–5984.

Vojtek, A. B., Hollenberg, S. M., and Cooper, J. A. (1993). Mammalian Ras interacts directly with the serine/threonine kinase Raf. Cell 74, 205–214.

Wagner, D. D., and Frenette, P. S. (2008). The vessel wall and its interactions. Blood 111, 5271–5281.

Zografou, S., Basagiannis, D., Papafotika, A., Shirakawa, R., Horiuchi, H., Auerbach, D., Fukuda, M., and Christoforidis, S. (2012). A complete Rab screening reveals novel insights in Weibel-Palade body exocytosis. J. Cell Sci. 125, 4780–4790.

Figure legends

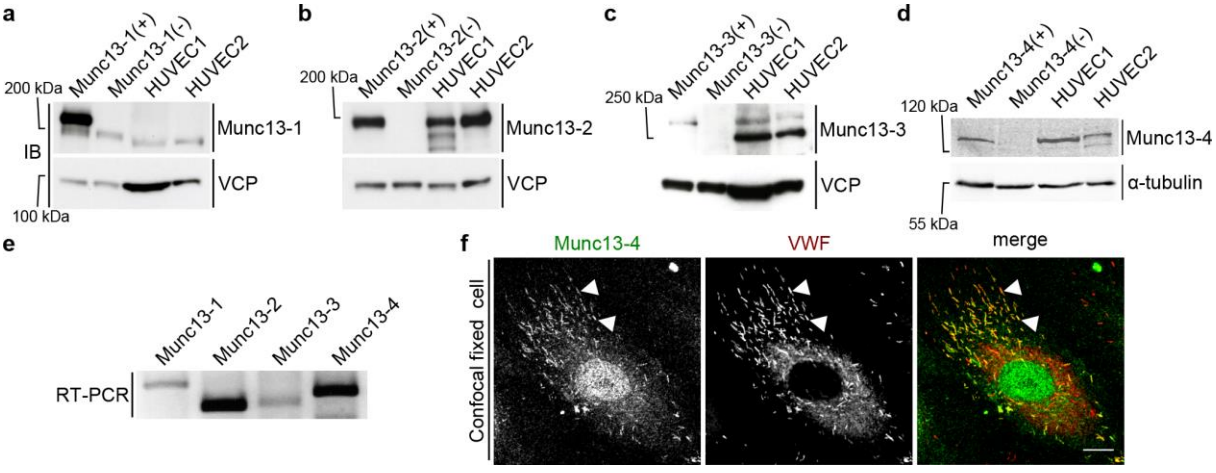

Figure 1. Expression and localization of Munc13 proteins in human endothelial cells.

(**a**-**d**) Western blot (IB) detection of Munc13-1 to -4 in two different HUVEC lysates. Included are positive (+) and negative controls (-), i.e. mouse brain lysates (Munc13-1 to -3) or mouse lung lysate (Munc13-4) from wildtype or the respective knockout mouse. Calculated molecular masses are: Munc13-1, 193 kDa; Munc13-2, 180 kDa; Munc13-3, 250 kDa (migrates at appr. 280kDa in SDS-PAGE(Varoqueaux *et al.*, 2005); Munc13-4, 123 kDa. VCP (97 kDa) and alpha-tubulin (55 kDa) served as loading control. In (**a**), the weaker band below Munc13-1 most likely corresponds to Munc13-2 which shows some cross-reactivity with the anti-Munc13-1 antibody (Cooper *et al.*, 2012). The lower band in the HUVEC lysates in panel (**c**) likely stems from an unspecific antibody reaction as it is not seen in the mouse lysates.

(**e**) Reverse transcription PCR (RT-PCR) of HUVEC cDNA with primers amplifying specific sequences of all human Munc13 proteins (Munc13-1, 243 bp; Munc13-2, 159 bp; Munc13-3, 168 bp; Munc13-4, 201 bp).

(**f**) Confocal section of fixed HUVEC labeled with anti-Munc13-4 and anti-VWF antibodies and AlexaFluor488- and AlexaFluor647-conjugated secondary antibodies. Arrowheads mark examples of colocalizations of Munc13-4 and VWF on WPBs. Scale bar represents 10 µm.

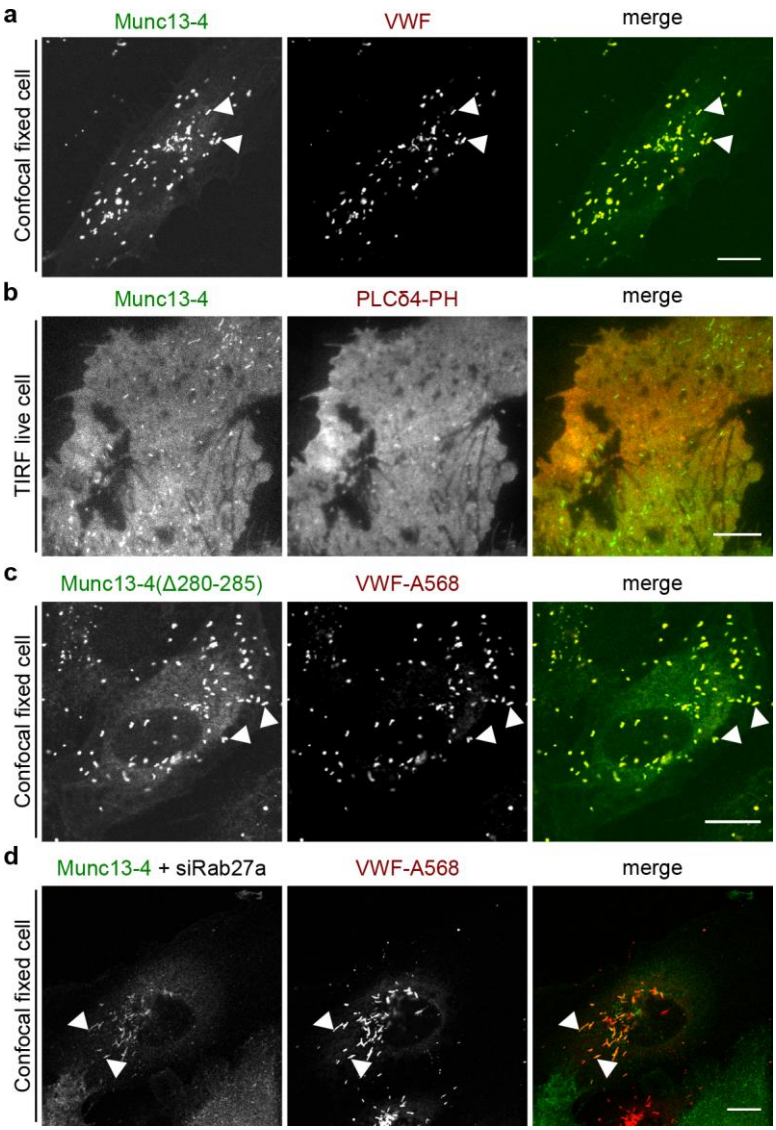

Figure 2. Munc13-4 localizes to WPBs and the plasma membrane independently of Rab27a.

(**a**) Confocal section of fixed HUVEC expressing YFP-Munc13-4 for 48 h and labeled with anti-VWF and AlexaFluor568-conjugated secondary antibodies.

(**b**) TIRF section of live HUVEC expressing YFP-Munc13-4 and the PI(4,5)P_2-binding domain PLCδ4-PH-mKate as membrane marker.

(**c**) Confocal section of fixed HUVEC expressing GFP-Munc13-4(Δ280-285), a mutant incapable of binding Rab27a, and labeled with anti-VWF and AlexaFluor568-conjugated secondary antibodies.

(**d**) Confocal section of fixed HUVEC expressing YFP-Munc13-4 and transfected with siRNA against Rab27a (siRab27a) for 48 h. Cells were labeled with anti-VWF and AlexaFluor568-conjugated secondary antibodies.

Arrowheads mark examples of colocalizations of Munc13-4 and VWF on WPBs. Scale bars represent 10 µm.

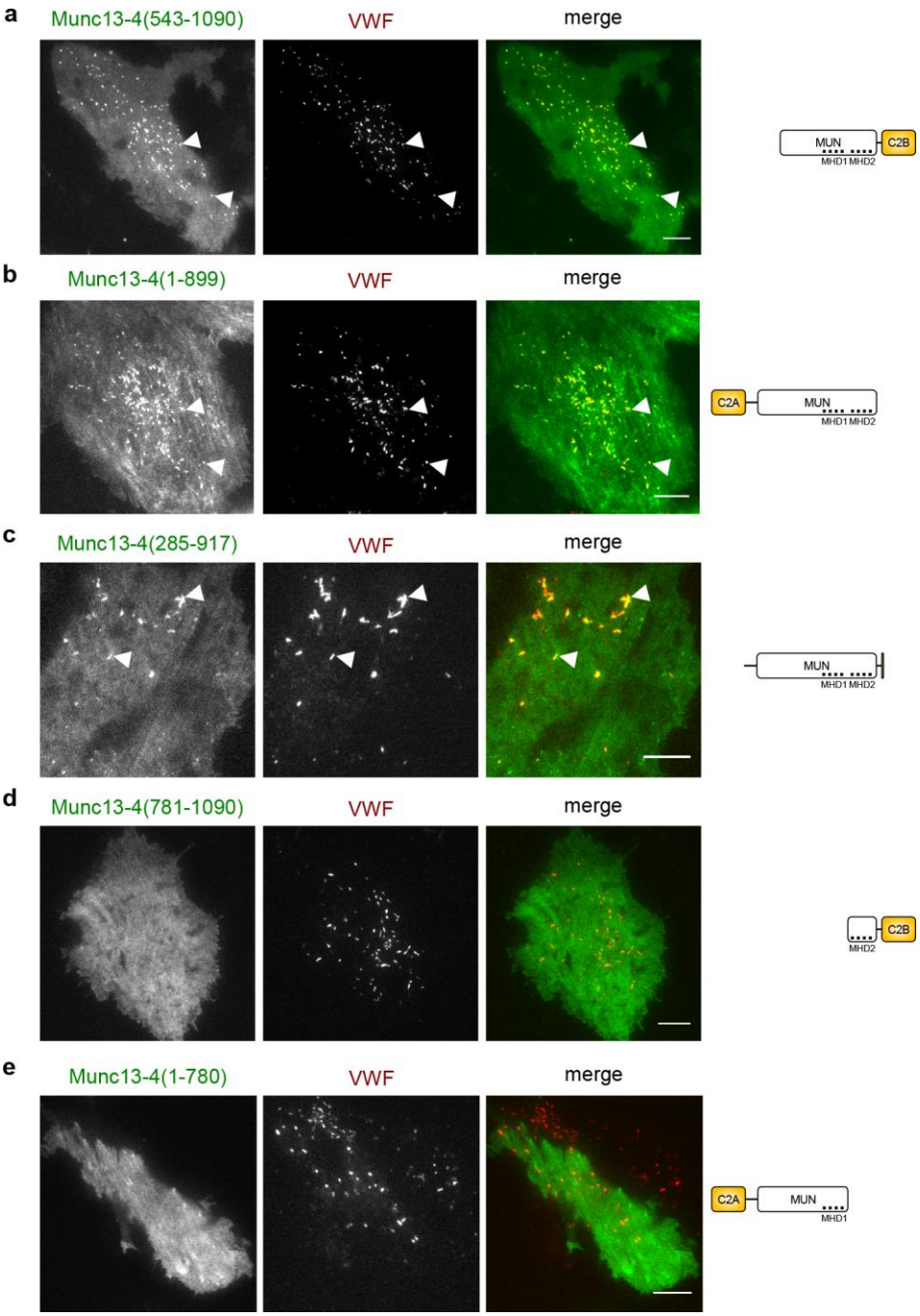

Figure 3. Munc13-4 localizes to WPBs via its MHD1/MHD2 region.

TIRF images of live HUVEC expressing different truncated versions of YFP-Munc13-4 and VWF-RFP as WPB marker for 48 h. On the right side, the domain structures of the respective Munc13-4 mutants lacking either the C2A (aa 109-284), C2B (aa 904-1047), or parts of the MUN domain (aa 319-901) are shown. The first about hundred amino acids of Munc13-4 of unknown structure were omitted for simplicity. MHD1 (aa 577-677) and MHD2 (aa 788-894) are two regions within the MUN domain with conserved sequences in all Munc13 proteins.

(**a**) Munc13-4(543-1090), which lacks the C2A and parts of MUN domain but contains the entire region around MHD1/2.

(**b**) Munc13-4(1-899), which lacks the C2B but contains the entire MHD1/2 region.

(**c**) Munc13-4(285-917), which lacks C2A and C2B.

(**d**) Munc13-4(1-780), which is truncated after MHD1 and therefore lacks MHD2-C2B.

(**e**) Munc13-4(781-1090), which lacks the entire N-terminal part including MHD1.

Arrowheads mark examples of colocalizations of Munc13-4 and VWF on WPBs. Note that mutants containing the MHD1 and MHD2 regions localize to WPBs, whereas those lacking these sequences do not. Scale bars represent 10 µm.

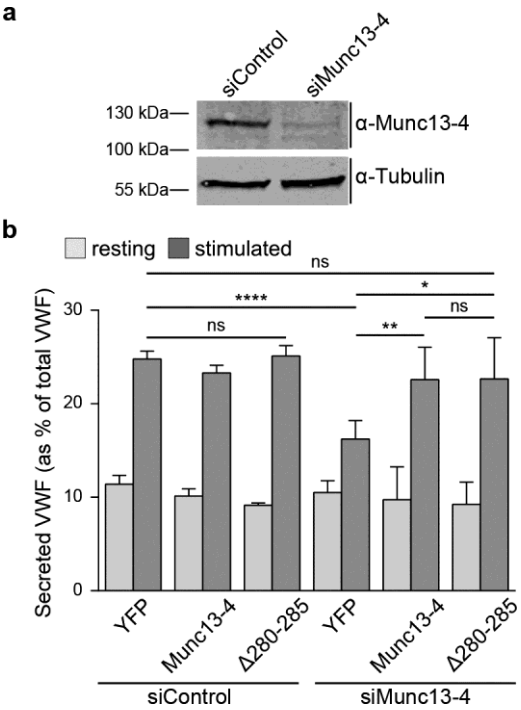

Figure 4. Munc13-4 is required for histamine-induced secretion of VWF.

(**a**) HUVEC were treated either with unspecific siRNA as control (siControl) or with siRNA targeting Munc13-4 (siMunc13-4), and lysates of the respective cells were subjected to Western blot analysis with anti-Munc13-4 antibodies. Probing with anti-alpha-Tubulin (55 kDa) antibodies served as loading control. Note that endogenous Munc13-4 was successfully depleted.

(**b**) ELISA-based VWF secretion assay. HUVEC were transfected with siControl or Munc13-4 targeting siRNA (siMunc13-4) plus expression vectors encoding YFP (control), YFP-Munc13-4 or GFP-Munc13-4(Δ280-285), which were both rendered insensitive to the specific Munc13-4 siRNA (see Materials and methods). In each case, the amount of VWF secreted into the cell culture supernatant was measured by ELISA. Shown are means of at least five independent experiments that were tested

for statistical significance by one-way ANOVA with Tukey's test (ns, not statistically significant, * p≤0.05, ** p≤0.01, **** p≤0.0001). Bars represent mean±SEM. The numbers of independent experiments n were as follows: siControl + YFP or Munc13-4, n=8; siControl + Δ280-285, n=7; siMunc13-4 + YFP or Munc13-4, n=6; siMunc13-4 + Δ280-285, n=5.

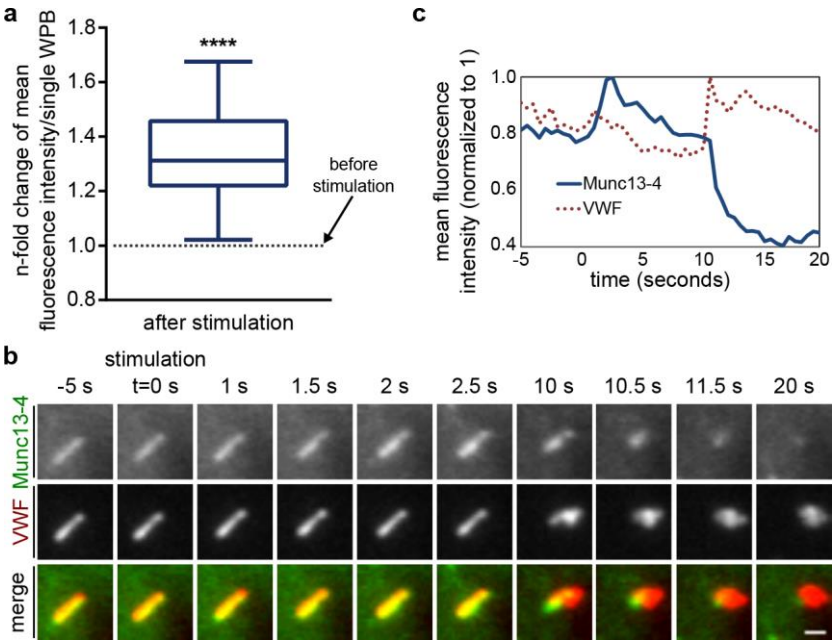

Figure 5. Histamine stimulation induces an additional recruitment of Munc13-4 to WPBs.

(**a**) Munc13-4 fluorescence signals increase on WPBs after histamine stimulation. Cells expressing YFP-Munc13-4 or Munc13-4-mKate together with VWF-RFP or VWF-GFP were stimulated with histamine and imaged by live-cell confocal microscopy. Image stills were thresholded in ImageJ to create regions-of-interest (ROIs) for Munc13-4-positive WPBs in a cell and to compare mean fluorescence intensities of all ROIs shortly before and shortly after stimulation. Mean fluorescence intensity before stimulation was set to 1 and the increase after stimulation was measured as the n-fold change in mean fluorescence intensity for every individual ROIs. Mean n-fold changes from all individual ROIs (a total of n=323 WPBs from at least three independent experiments) were tested for statistical significance by one-sample t-test (**** p≤0.0001).

(**b**) Munc13-4 increases and then disappears at WPB during exocytosis. HUVEC expressing YFP-Munc13-4 and VWF-RFP were stimulated with 100 µM histamine and the fusion of individual WPBs with the plasma membrane was recorded by TIRF microscopy. Shown are TIRF sections of a single WPB positive for YFP-Munc13-4

and VWF-RFP. The cell was stimulated at t=0 s and fusion of this WPB occurred at t=10 s. See also supplementary video Fig5video01. Scale bar represents 1 µm.

(**c**) Graph depicting the corresponding mean fluorescence intensities (YFP, RFP) of the WPB shown in (**b**) over time. The YFP-Munc13-4 signature shows a fluorescence increase upon stimulation (t=0 s to t=2.5 s), and subsequently a rapid decrease in fluorescence that coincides with the formation of a characteristic VWF fusion spot (t=10 s to t=11.5s).

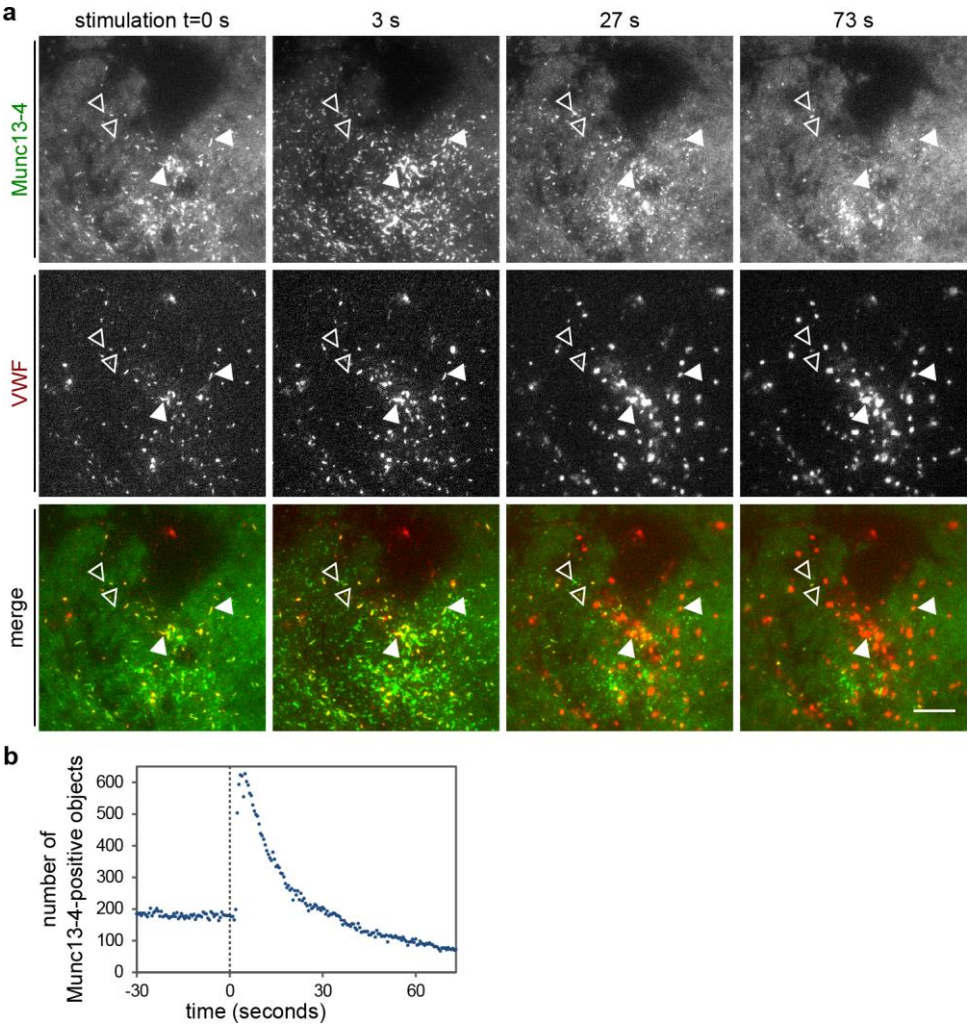

Figure 6. Histamine stimulation induces a clustering of Munc13-4 at or close to the plasma membrane.

(**a**) TIRF sections of live HUVEC expressing YFP-Munc13-4 and VWF-RFP as WPB marker and stimulated with 100 µM histamine at t=0 s. Before stimulation, YFP-Munc13-4 shows a general plasma membrane localization and is present on VWF-RFP-positive WPBs that reside in the TIRF field (examples marked by filled arrowheads). Some YFP-Munc13-4-positive objects that are shaped like WPBs but do not contain VWF-RFP can also be weakly seen against the general background (examples marked by open arrowheads). Stimulation triggers an additional clustering

of Munc13-4 (t=3 s), i.e. the Munc13-4-positive objects become brighter as more Munc13-4 is recruited to them (see also Fig. 5 for WPB-associated Munc13-4). WPB exocytosis, which is accompanied by the formation of a characteristic VWF-RFP fusion spot, leads to a disappearance of the Munc13-4-positive clusters. Arrowheads mark examples of Munc13-4-positive objects that colocalize with VWF-RFP and disappear following WPB fusion (fusion here occurred between t=3 and t=27 s). Scale bar represents 10 µm. See also supplementary video Fig6video02.

(**b**) Graph displaying the number of Munc13-4-positive objects over time per cell in the TIRF field.

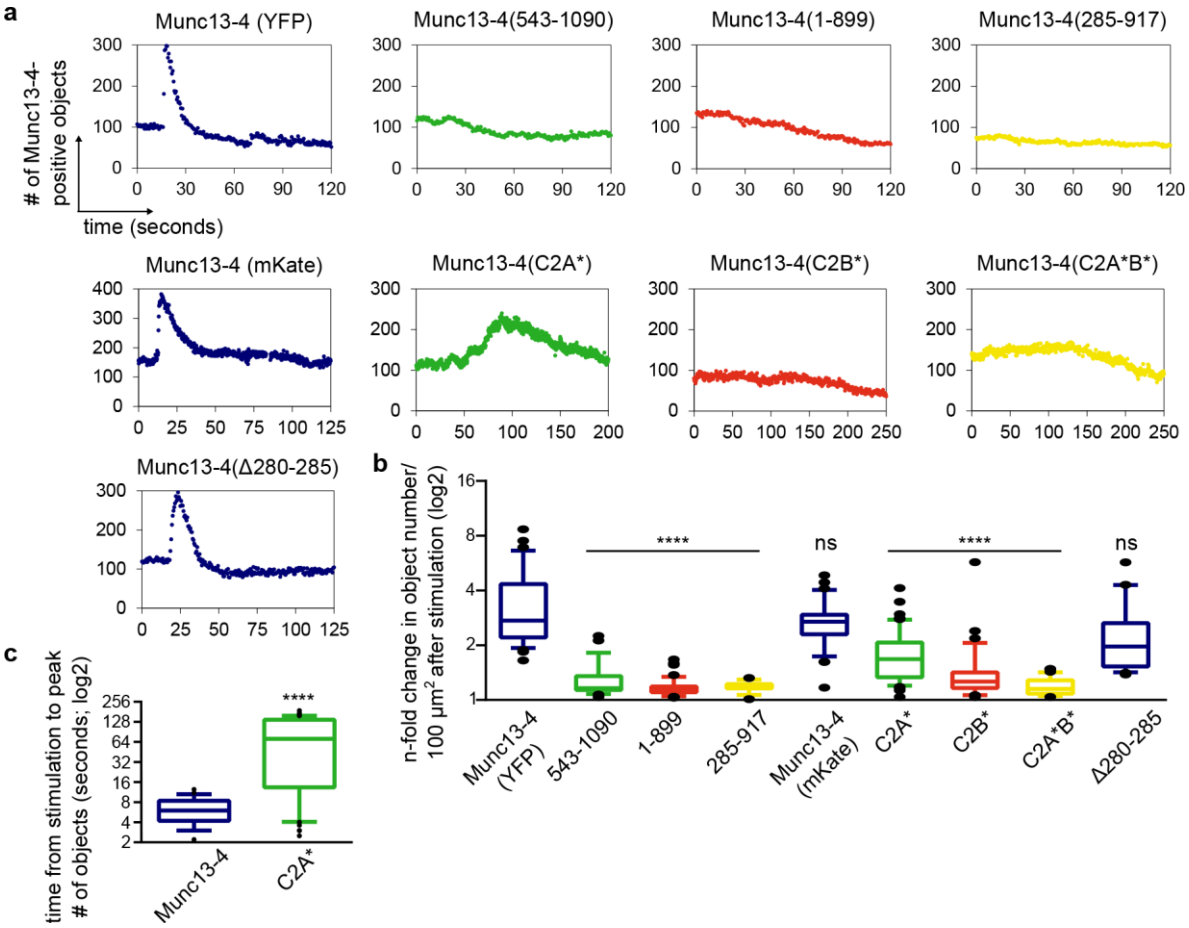

Figure 7. Deletion of C2A or C2B abolishes the stimulation-induced clustering of Munc13-4 at the plasma membrane.

TIRF time-lapse movies of live HUVEC expressing YFP-Munc13-4, Munc13-4-mKate or the indicated mutant constructs and VWF-RFP as WPB marker were recorded and the obtained images subsequently analyzed by the object detection algorithm MorphoQuant.

(**a**) Representative graphs showing the number of Munc13-4-positive objects detected in the TIRF field of HUVEC stimulated with 100 µM histamine at t=15 s.

Cells were transfected with YFP- or mKate-tagged full-length Munc13-4, Munc13-4 variants with truncated C2 domains, Munc13-4 variants with mutations in the Ca^{2+}-binding sites of the C2 domains, or Munc13-4(Δ280-285). Munc13-4(543-1090) lacks the C2A domain, Munc13-4(1-899) lacks the C2B domain and Munc13-4(285-917) lacks both C2A and C2B (Elstak *et al.*, 2011). Munc13-4(C2A*) carries two point mutations in the Ca^{2+}-binding site of the C2A domain, Munc13-4(C2B*) carries two analogous point mutations in the Ca^{2+}-binding site of the C2B domain, and Munc13-4(C2A*B*) carries these mutations in both C2 domains (Boswell *et al.*, 2012).

(**b**) Change in the number of Munc13-4-positive objects per 100 μm^2 after histamine stimulation. Cells were transfected and stimulated as in (a). Means of n-fold changes over all cells from at least 5 independent experiments were tested for statistical significance by one-way ANOVA with Tukey's test (ns, statistically not significant, **** $p \leq 0.0001$, as compared to the wildtype samples). Numbers of cells analyzed, n, were as follows: Munc13-4, n=33; Munc13-4(543-1090), n=27; Munc13-4(1-899), n=42; Munc13-4(285-917), n=14; Munc13-4, n=32; Munc13-4(C2A*), n=52; Munc13-4(C2B*), n=35; Munc13-4(C2A*B*), n=35. Means±SEM: 3.5±0.3/1.3±0.03/1.2±0.02/1.2±0.02/ 2.8±0.1/1.8±0.1/1.5±0.1/1.2±0.02 /2.3±0.2.

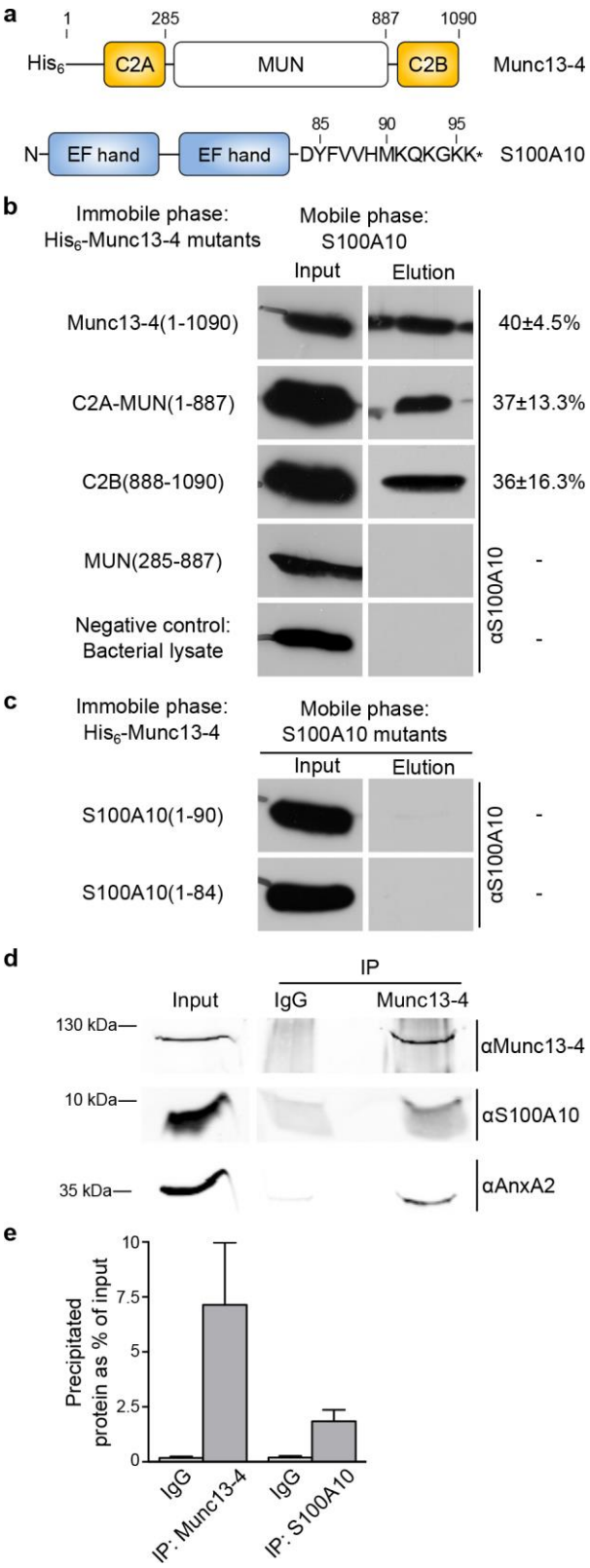

Figure 8. Munc13-4 interacts with the S100A10 subunit of the AnxA2-S100A10 complex.

(**a**) Domain structures of Munc13-4 and S100A10. MUN, Munc13-homology domain. (**b**) S100A10 binds to both C2 domains of Munc13-4. In vitro binding assay with full-length or truncated mutants of Munc13-4 and wild-type S100A10. Bacterially

expressed His_6-Munc13-4 derivatives were immobilized on NiNTA and incubated with purified S100A10 (Input). After several washing steps, bound S100A10 was eluted as described in Materials and methods (Elution). Lysates of untransformed *E. coli* served as negative control. The amount of eluted S100A10 as percent of S100A10 input was quantified from at least three different expreriment and is given next to the respective mutant panel on the right. Values are means±SEM.

(**c**) Two C-terminally truncated mutants of S100A10, S100A10(1-90) and S100A10(1-84), do not bind Munc13-4. In vitro binding assay as described in (**b**) with immobilized full-length His_6-Munc13-4 and the two S100A10 truncation mutants. Note that S100A10(1-90) which can still bind AnxA2(Kube *et al.*, 1992) fails to interact with Munc13-4.

(**d**) Co-immunoprecipitation of Munc13-4 and AnxA2-S100A10. Postnuclear HUVEC supernatants were incubated with dynabead-coupled antibodies against either Munc13-4 (IP Munc13-4) or rabbit IgGs as negative control (IP IgG). The starting material (Input) and the precipitated proteins were analyzed by SDS-PAGE (15% gel in upper, 10% gel in lower panels) and immunoblotting with antibodies against Munc13-4, S100A10 or AnxA2.

(e) Relative amount of precipitated Munc13-4 and S100A10 in the immunoprecipitation experiments using either specific anti-Munc13-4 (IP) or control rabbit IgGs (IgG). Band intensities were calculated as percent of the input material from five independent experiments (one example is shown in figure 8d). Bars represent mean±SEM.

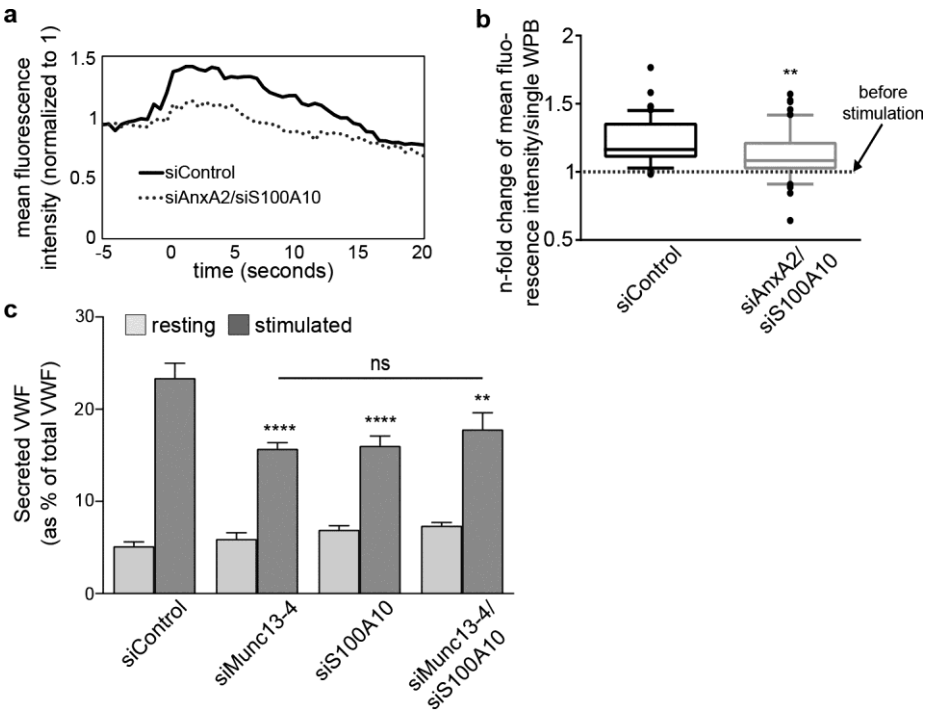

Figure 9. Munc13-4 and S100A10 function together in histamine-induced secretion of VWF.

(a, b) Histamine-induced recruitment of Munc13-4 to WPB fusion sites is decreased upon AnxA2-S100A10 depletion. HUVEC were tansfected for 48 h with VWF-GFP as WPB marker, Munc13-4-mKate and unspecific siControl RNAs or siRNAs targeting AnxA2-S100A10. Cells were stimulated with histamine at t=0 s, imaged by live-cell TIRF microscopy and individual WPB fusion sites were identified by a collapse of the VWF-GFP signal. Image stills were thresholded in ImageJ to create regions-of-interest (ROIs) for Munc13-4-positive WPBs at WPB fusion sites and to compare mean fluorescence intensities of all ROIs shortly before and shortly after stimulation. Mean fluorescence intensity before stimulation was set to 1 and the increase after stimulation was measured as the n-fold change in mean fluorescence intensity. (a) Examples of Munc13-4-mKate mean fluorescence intensity recordings of individual WPBs from cells treated with siControl or siRNAs targeting AnxA2-S100A10, respectively. (b) Comparison of histamine-induced Munc13-4-mKate fluorescence intensity changes of individual WPBs in siControl and siAnxA2/siS100A10 treated cells at 2.5 s after stimulation. Mean n-fold changes from individual ROIs for Munc13-4-mKate positive WPBs (a total of at least n=57 WPBs per condition from at least three independent experiments) were tested for statistical significance by Mann-Whitney U test (** $p \leq 0.01$).

(c) ELISA-based VWF secretion assay. HUVEC were transfected for 48 h with unspecific siControl or siRNA targeting Munc13-4 (siMunc13-4) or S100A10 (siS100A10), or siRNAs targeting both proteins in a double knockdown (siMunc13-4/siS100A10). In each case, the amount of VWF secreted into the cell culture supernatant was measured by ELISA. Shown are means of four independent experiments that were tested for statistical significance by one-way ANOVA with Tukey's test (** $p \leq 0.01$, *** $p \leq 0.001$, **** $p \leq 0.0001$ as related to the control sample). Differences between samples treated with specific siRNA were statistically not significant (ns). Bars represent mean±SEM.